CaMKII is a novel regulator of diacylglycerol lipase-α and striatal endocannabinoid signaling

Brian C. Shonesy[1], Xiaohan Wang[2,3], Kristie L. Rose[4], Teniel S. Ramikie[2,5], Victoria S. Cavener[2], Tyler Rentz[1], Anthony J. Baucum II[1], Nidhi Jalan-Sakrikar[1], Ken Mackie[7], Danny G. Winder[1,2,6], Sachin Patel[1,2,5,6*], Roger J. Colbran[1,2,6*]

[1]Department of Molecular Physiology and Biophysics,
[2]Vanderbilt Brain Institute,
[3]Vanderbilt International Scholar Program,
[4]Department of Biochemistry,
[5]Department of Psychiatry,
[6]Vanderbilt-Kennedy Center for Research on Human Development,
Vanderbilt University School of Medicine, Nashville, TN, USA

[7]The Gill Center and the Department of Psychological & Brain Sciences, Indiana University, Bloomington, IN, USA

Supplementary Materials

Supplementary Tables 1-2

Supplementary Figures 1-7

Supplemental Table 1. Proteins identified in DGLα immune complexes isolated from mouse striatum. DGLα was immunoprecipitated from a mouse striatal extract and analyzed by LC/MS/MS. The table lists UNIPROT accession numbers of the proteins identified, along with gene and protein names, the percent coverage and the number of spectral counts. This listing excludes common contaminants (i.e., mouse/human keratin).

Accession Number	Gene Name	Protein Name	Coverage (%)	Spectral Counts
P11798	Camk2a	Calcium/calmodulin-dependent protein kinase type II subunit alpha	39	25
Q62108	Dlg4	Postsynaptic density protein 95 (PSD95)	37	22
Q4ACU6	Shank3	SH3 and multiple ankyrin repeat domains protein 3 (Shank3)	19	22
P28652	Camk2b	Calcium/calmodulin-dependent protein kinase type II subunit beta	36	19
A4FU75	Dagla	Diacylglycerol lipase alpha	15	17
P60710	Actb	Actin, cytoplasmic 1 (β-actin)	38	15
Q9Z2Y3	Homer1	Homer protein homolog 1	34	14
P62737	Acta2	Actin, aortic smooth muscle (α-actin-2)	25	12
P99024	Tubb5	Tubulin beta-5 chain	22	12
Q7TMM9	Tubb2a	Tubulin beta-2A chain	19	11
B1AZ43	Baiap2	Brain-specific angiogenesis inhibitor 1-associated protein 2	19	9
Q91XM9	Dlg2	Postsynaptic density protein PSD-93	10	6
P68373	Tuba1c	Tubulin alpha-1C chain	18	6
Q6PFD5	Dlgap3	PSD-95/SAP90-binding protein 3 (SAPAP3)	8	6
P68368	Tuba4a	Tubulin alpha-4A chain	16	5
D2KHZ9	Gapdh	Glyceraldehyde-3-phosphate dehydrogenase	21	5
P51881	Slc25a5	ADP/ATP translocase 2	17	4
P19246	Nefh	Neurofilament heavy polypeptide	2	3
A4GZ26	Iqsec2	ARF6 guanine nucleotide exchange factor (IQArfGEF)	2	3
Q8R0S2	Iqsec1	IQ motif and SEC7 domain-containing protein 1	3	3
P08551	Nefl	Neurofilament light polypeptide	5	3
Q8BJ42	Dlgap2	PSD-95/SAP90-binding protein 2 (SAPAP2)	2	2
Q03265	Atp5a1	ATP synthase subunit alpha, mitochondrial	5	2
Q3U6C7	Sucla2	Succinyl-CoA ligase [ADP-forming] subunit beta, mitochondrial	4	2
P17897	Lyz1	Lysozyme C-1	14	2
Q8BIZ1	Anks1b	Ankyrin repeat and sterile alpha motif domain-containing protein 1B	2	2

Supplementary Table 2. Target peptides and selected transitions for MRM analysis. For detailed explanation see Experimental Methods.

Peptide Sequence	Modification State	Precursor		Collision Energy	Product		
		m/z	Charge		m/z	Charge	Ion
GSPSLHAVLER	unmodified	583.3198	2	20	417.2456	1	y3
		583.3198	2	20	516.3140	1	y4
		583.3198	2	20	587.3511	1	y5
		583.3198	2	20	724.4100	1	y6
		583.3198	2	20	511.2931	2	y9
GSPSLHAVLER	pSer 808	623.3030	2	22	417.2456	1	y3
		623.3030	2	22	516.3140	1	y4
		623.3030	2	22	587.3511	1	y5
		623.3030	2	22	724.4100	1	y6
		623.3030	2	22	551.2763	2	y9
		623.3030	2	22	502.2878	2	y9-H_3PO_4
RAPLATMESLSDTESLYSFDSR	unmodified	826.0602	3	34	524.2463	1	y4
		826.0602	3	34	611.2784	1	y5
		826.0602	3	34	774.3417	1	y6
		826.0602	3	34	887.4258	1	y7
		826.0602	3	34	974.4578	1	y8
RAPLATMESLSDTESLYSFDSR	pSer 782	852.7156	3	35	524.2463	1	y4
		852.7156	3	35	611.2784	1	y5
		852.7156	3	35	774.3417	1	y6
		852.7156	3	35	887.4258	1	y7
		852.7156	3	35	974.4578	1	y8

Supplemental Figure 1. Original unmodified images used to generate figures. **(a)** Images of the entire CaMKII blots that were cropped to generate Fig. 1d. The Non-Phos and P-T286 samples were analyzed in parallel on separate blots, and the films were exposed for the identical time. **(b)** Protein stain and ^{32}P autoradiograph of the entire gel that was cropped to generate Fig. 2g. Autophosphorylation of CaMKII resulted in the ≈50 kDa band indicated on the autoradiograph. **(a,b)** BSA was included in these assays, and is indicated.

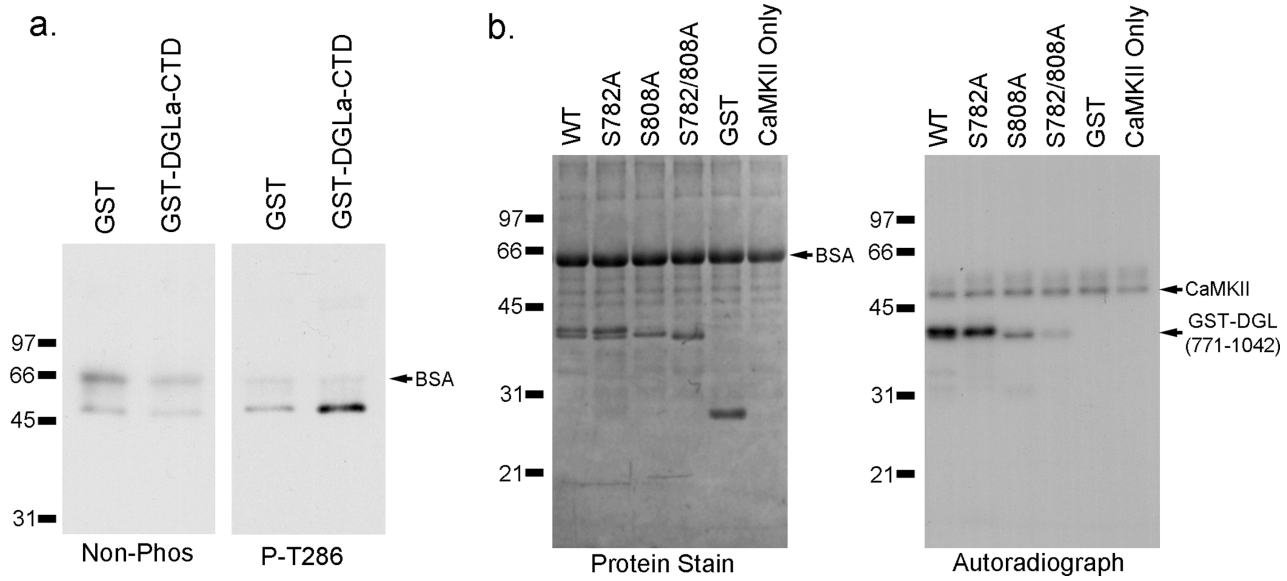

Supplemental Figure 2. CaMKIIα is autophosphorylated at Thr286 in HEK293 cells. HEK293 cells expressing WT CaMKIIα or T286A-CaMKIIα were lysed for analysis by western blot using antibodies to total CaMKIIα or to phospho-Thr286 CaMKIIα. The WT protein is significantly autophosphorylated under these basal culture conditions, consistent with prior reports (Jalan-Sakrikar et al., 2011).

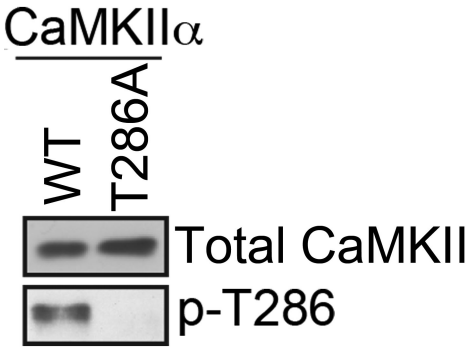

Supplementary Figure 3. Chromatographic profiles following MRM analysis of phosphorylated DGLα peptides 805–815 (GSPSLHAVLER, **a–c**) and 774–795 (RAPLATMESLSDTESLYSFDSR, **d–f**) from HEK293T cells. **(a, d)** Tryptic peptides derived from GST-DGLα(761–870) phosphorylated *in vitro* by CaMKIIα at Ser^{808} and Ser^{782} (Fig. 2) were used as peptide standards for MRM method development. Chromatographic profiles are shown for the transition intensities observed upon targeted analysis of the two phosphorylated peptides. The intensities for each product ion monitored are plotted over time as the targeted precursor peptide is eluted into the mass spectrometer for analysis. The retention time at the peak apex of the most intense transition is provided for each peptide analyzed. The peptide sequence provided above each set of data is indicated with the specific y-type product ions that were selected for monitoring, and the brackets denote the positions of peptide backbone cleavage events that generate these product ions. Each bracket color represents a single monitored product ion or transition, and the co-eluting chromatographic profiles for each transition are similarly color-coded. **(b, c, e, f)** Identical analysis of phosphorylated full length DGLα purified from lysates of HEK293T cells with **(b, e)** or without **(c, f)** co-expression of constitutively active CaMKIIα. The non-phosphorylated forms of both peptides displayed similar relative intensities of individual transitions and were detected at similar levels in (–) and (+) CaMKIIα conditions.

In panel **(a)**, MRM analysis of *in vitro* phosphorylated DGLα identified phosphorylation at Ser^{808} unambiguously. The DGLα tryptic 805–815 peptide fragments in such a manner that enables monitoring of the y_9 product ion as well as the H_3PO_4 neutral loss y_9 product ion. The presence of these specific y_9 transitions, in combination with y_3-y_6 allows for specific identification of Ser^{808} as the phosphorylated residue. In comparison to panel **(a)**, MRM analysis of full length DGLα from HEK293T cells confirms the presence of the Ser^{808} phosphorylated peptide after co-expression with CaMKIIα (**b**); note the similar relative intensities of individual transition peaks, and the similarity in retention time of the co-eluting transition profiles. In the absence of co-expressed CaMKIIα (**c**), the transition intensities for this peptide in the full length DGLα preparation were relatively low, and the presence of the Ser^{808}-phosphorylated peptide could not be confirmed in this preparation.

In panel **d**, the fragmentation characteristics of the phosphorylated DGLα peptide 774–795 enabled monitoring of product ions, y_4–y_8. The mass of the precursor peptide in combination with the detection of these particular ions confirms the presence of phosphorylated DGLα 774–795, and also indicates that phosphorylation must be on one of the four N-terminal Ser or Thr residues. Independent experiments unambiguously identified Ser^{782} as the phosphorylation site (Fig. 2). In panel **e**, the co-eluting transition profiles at the same retention time in the analysis of DGLα co-expressed with CaMKIIα validate the identification of phosphorylated 774–795 peptide, and suggest that Ser^{782} is phosphorylated by CaMKIIα in intact 293T cells. In contrast, the presence of this phosphorylated peptide was not confirmed upon analysis of DGLα purified from HEK293T cells that were not co-transfected with CaMKIIα.

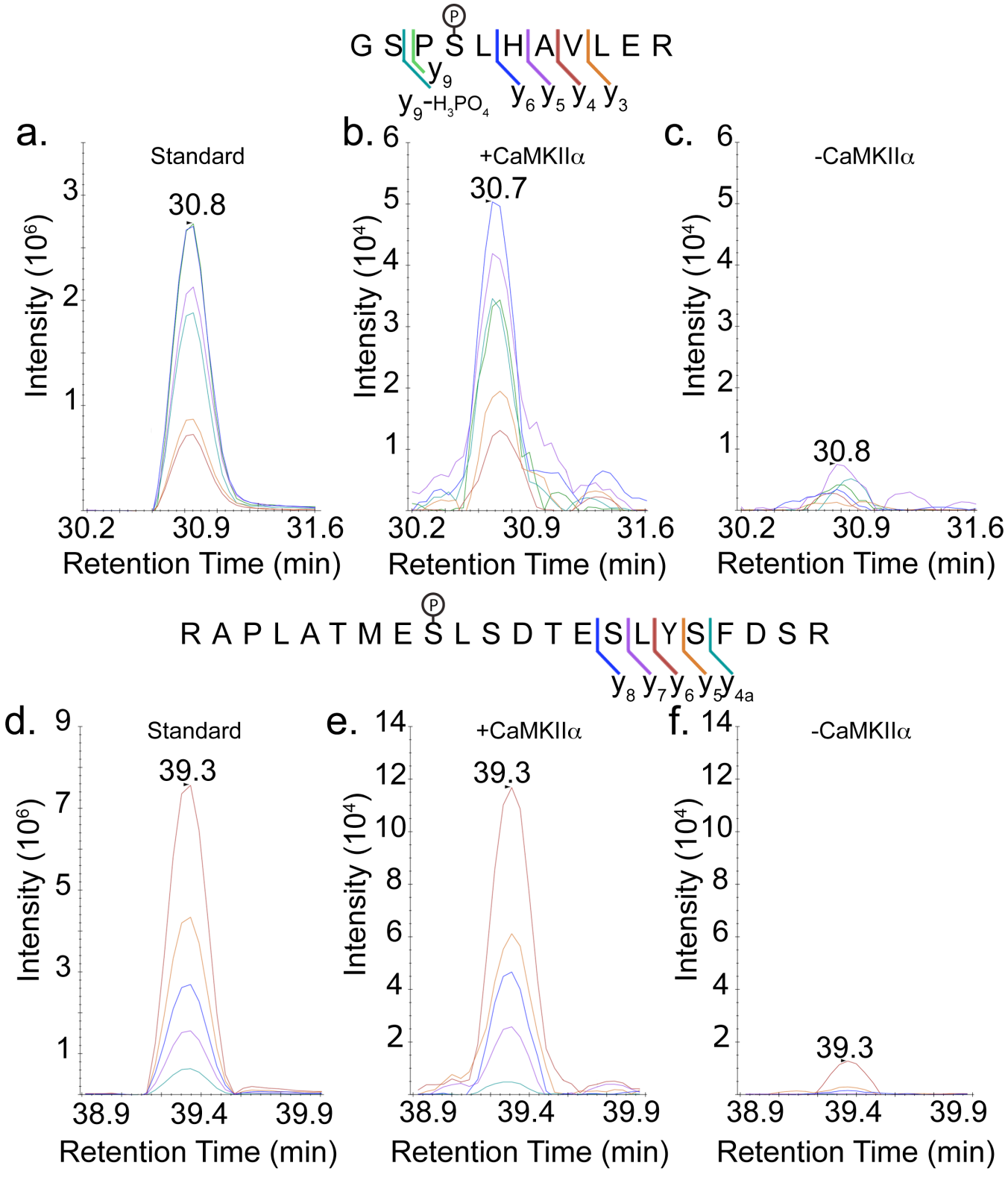
G S P S L H A V L E R
P
y9
y9-H3PO4
y6 y5 y4 y3
a.
Standard
30.8
Intensity (10^6)
Retention Time (min)
b.
+CaMKIIα
30.7
Intensity (10^4)
Retention Time (min)
c.
-CaMKIIα
30.8
Intensity (10^4)
Retention Time (min)
R A P L A T M E S L S D T E S L Y S F D S R
P
y8 y7 y6 y5 y4a
d.
Standard
39.3
Intensity (10^6)
Retention Time (min)
e.
+CaMKIIα
39.3
Intensity (10^4)
Retention Time (min)
f.
-CaMKIIα
39.3
Intensity (10^4)
Retention Time (min)

Supplemental Figure 4. Basic characterization of the DGL activity assay. **(a)** Time course of DGL activity in striatal membranes following addition of SAG (250 μM) is approximately linear up to 30 min. **(b)** SAG concentration-dependence of 2-AG production at 15 min by striatal membranes in the presence of vehicle (black) or tetrahydrolipstatin (THL; 1 μM; gray), a DGL inhibitor. THL inhibited 2-AG production as analyzed by 2-way ANOVA: Interaction $F_{3,6}$=179.3 p<0.0001, SAG $F_{3,6}$=409.7 p<0.0001, Drug $F_{1,2}$=863.5 p=0.0012; n=3 independent experiments), demonstrating that DGL was responsible for the majority of 2-AG production.

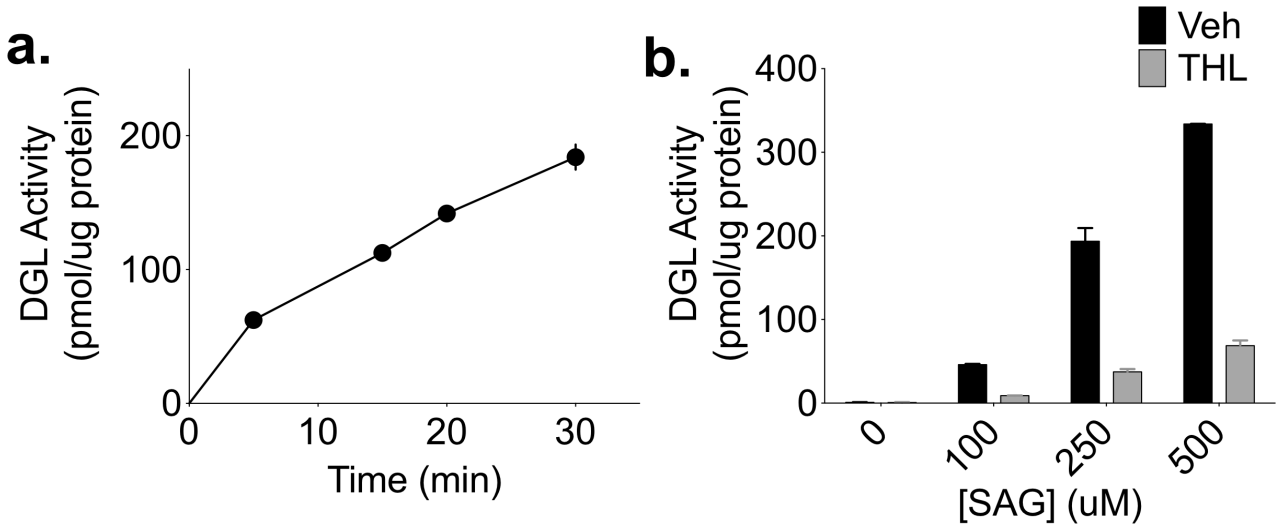

Supplemental Figure 5. Characterization of striatal DSE in direct and indirect pathway MSNs. **(a)** Representative DSE experiment in a randomly selected vehicle-treated MSN is shown. **(b,c)** Summary of average inhibition of eEPSCs by the DSE protocol in vehicle- and rimonabant-treated randomly selected MSNs (Veh 68±4%, n=8 cells from 1 mouse; rimonabant 94±2%, n=6 cells from 1 mouse; analyzed by unpaired two-tailed t-test (t_{12}=5.566, ### p=0.0001). **(d-g)** Effects of different durations of depolarization to induce DSE in **(d,e)** D2(–) and **(f,g)** D2(+) MSNs. Depression was determined by comparing to baseline (100%) by one sample t-test: D2(–) 2 sec: 99±4%, t_3=0.3964, p=0.7183, n=4 cells from 1 mouse; 3 sec: 86±1%, t_4=7.915, **p=0.0014, n=5 cells from 1 mouse; 5 sec: 79±6%, t_5=3.773, *p=0.0130, n=6 cells from 2 mice; 10 sec: 74±2%, t_{14}=10.48, ***p<0.0001, n=15 cells from 4 mice; D2(+) 2 sec: 92±4%, t_4=1.911, p=0.1286, n=5 cells from 1 mouse; 3 sec: 91±2%, t_4=3.029, p=0.0388, n=5 cells from 2 mice; 5 sec: 77±4%, t_6=6.005, 0.0010, n=7 cells from 2 mice; 10 sec: 67±2%, t_{14}=15.38, p<0.0001, n=15 cells from 4 mice. Representative traces are shown for each depolarization time. Calibration bars 20 ms x 150 pA.; * p<0.05, ** p<0.01, *** p<0.001

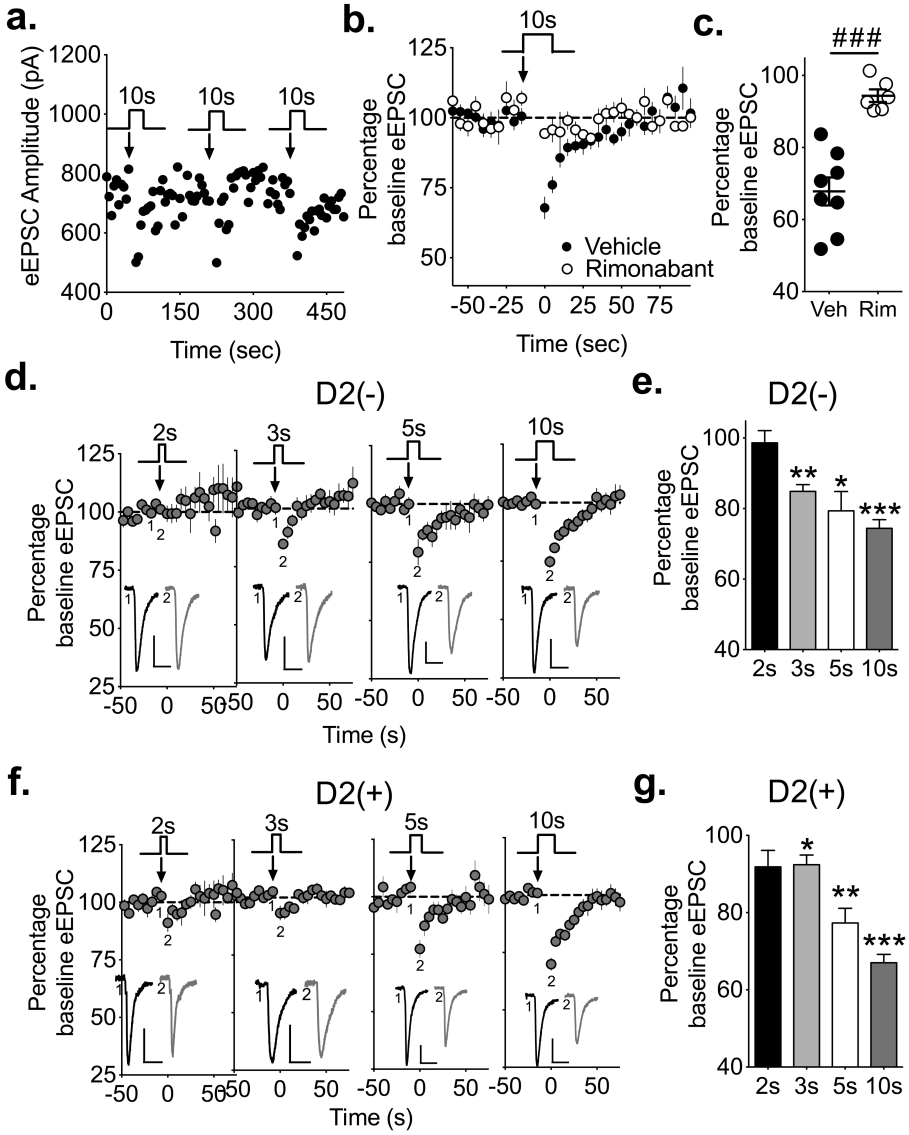

Supplemental Figure 6. Comparison of DSE in WT and CaMKIIα$^{T286A/T286A}$ (KI) MSNs following pretreatment of slices with DHPG (10 μM). **(a-d)** DHPG pretreatment prevented differences in DSE in **(a,b)** D2(–) MSNs from WT and KI mice with 3 s depolarization (WT 77±1%, n=9 cells from 3 mice; KI 78±3%, n=6 cells from 3 mice). **(c,d)** Addition of DHPG did not reveal differences in DSE between D2(+) MSNs from WT and KI mice with 3 s depolarization (WT 82±3%, n=9 cells from 3 mice; KI 80±3%, n=6 cells from 3 mice). Calibration bars 20 ms x 150 pA. **(e,f)** Comparison of DSE in D2(–) MSNs with and without postsynaptic loading of AIP (10 μM) following pretreatment of slices with DHPG (10 μM). **(e,f)** AIP had no effect on DSE when loaded into WT D2(–) MSNs pretreated with DHPG following 3s depolarization (79.1±2%, n=6 cells from 2 mice). Data from WT+DHPG cells are identical to WT cells in panels a and b and are replotted here for comparison. **(g)** Comparison of CB1R-agonist induced depression in WT and KI mice. The CB1R agonist WIN55,212-2 produced a similar depression in both WT and KI mice (WT = 55 ± 4, n=8 cells from 7 mice; KI = 53 ± 1, n=5 cells from 5 mice).

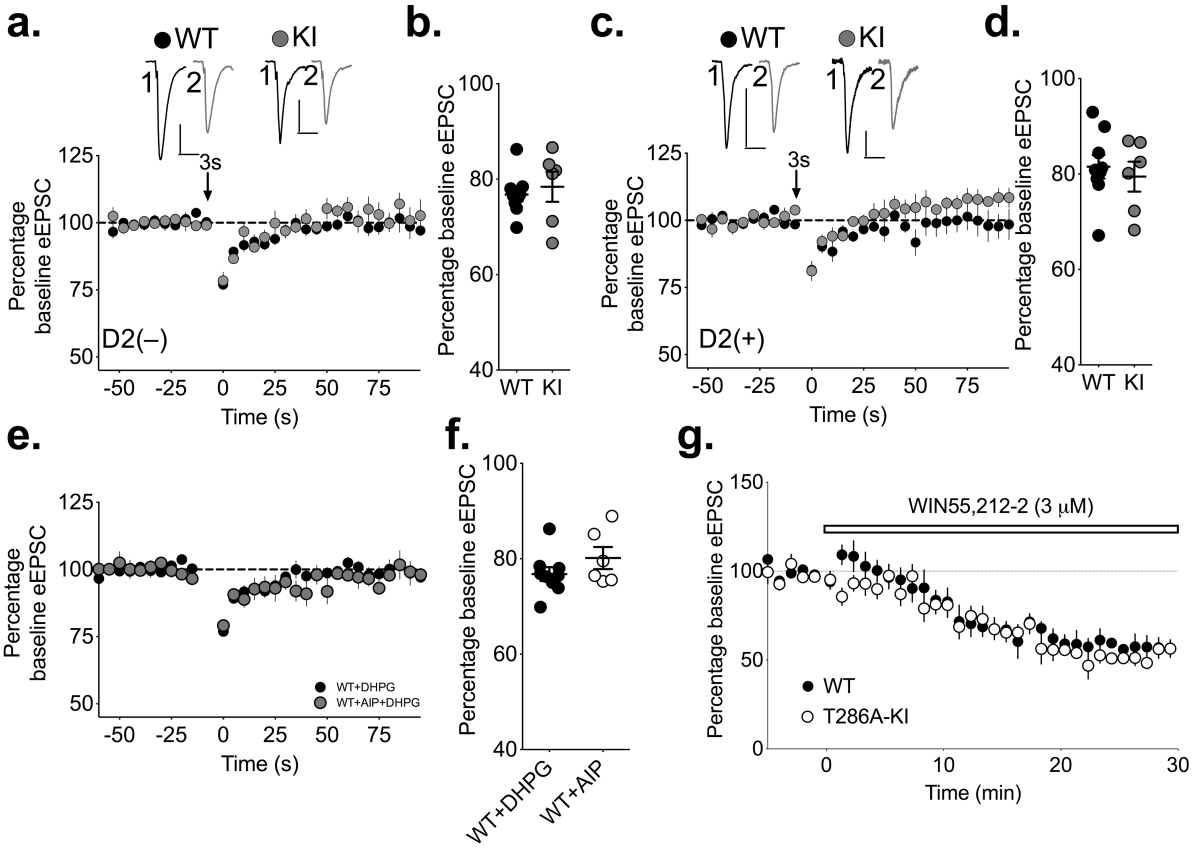

Supplementary Figure 7. Home cage monitoring of distance traveled by WT and CaMKII$\alpha^{T286A/T286A}$ (KI) mice over 60 hours. Unlike mice used for the experiment in Fig 5, these mice were not habituated to being singly housed in the same cage they were monitored in. The mice were placed in clean cages and monitoring began immediately. No drugs were administered to these mice. A period of habituation can be seen during the first few hours of the first night. This demonstrates that the mice are fully habituated within 24 hours and that both genotypes maintain a regular circadian locomotor activity pattern for at least 60 hours.